ISSN 1063-7842, Technical Physics, 2013, Vol. 58, No. 10, pp. 1481–1488. © Pleiades Publishing, Ltd., 2013.
Original Russian Text © A.K. Vershovskii, S.P. Dmitriev, A.S. Pazgalev, 2013, published in Zhurnal Tekhnicheskoi Fiziki, 2013, Vol. 83, No. 10, pp. 90–97.

OPTICS

Optically Pumped Quantum Magnetometer with Combined Advantages of M_X and M_Z Devices

A. K. Vershovskii*, S. P. Dmitriev, and A. S. Pazgalev

Ioffe Physical Technical Institute, Russian Academy of Sciences, Politekhnicheskaya ul. 26, St. Petersburg, 199034 Russia
**e-mail: antver@mail.ioffe.ru*

Received January 24, 2012; in final form, January 31, 2013

Abstract—A scheme of the magnetometer that simultaneously employs M_X and M_R magnetic resonance signals with the latter signal related to the radial component of the rotating atomic magnetic moment is proposed and tested. With respect to the shape, dynamic characteristics, and metrological parameters, the M_R signal is similar to the M_Z signal that is widely used in magnetometry but the former signal can be detected simultaneously with the M_X signal using a common radio optical scheme. The proposed device represents a fast M_X magnetometer with the phase in the feedback loop that is controlled by a slow precise M_R magnetometer implemented using the same atoms. The device that can be based on a conventional M_X sensor simultaneously exhibits a relatively short response time ($\tau \le 0.1$ s) and the accuracy that is approximately equal to the resolution of the quantum M_X discriminator at times of 10–100 s. The scheme is experimentally tested, and the statistic estimate of reproducibility is (1.2 ± 1.1) pT.

DOI: 10.1134/S1063784213100290

INTRODUCTION

Optically pumped quantum magnetometers (OPQMs) were proposed in the 1960s. The first comprehensive review can be found in [1] and recent results are summarized in [2, 3]. OPQMs can be used in fundamental physics in the high-accuracy experiments and in the applied measurements in magnetic geological survey, archeology, medicine, military science, etc. The OPQMs are based on the optical pumping [4, 5] and optical detection [6] of the magnetic resonance. In the simplest OPQM, polarized light induces optical orientation of the atoms with an intrinsic magnetic moment, so that the macroscopic magnetization of the medium is generated. The measured signal is a variation in the intensity of the resonant radiation having passed through the cell with the working substance.

In laboratory coordinates XYZ with the Z axis directed along the magnetic field, the vector of magnetic moment M moves along the surface of the Bloch sphere under the conditions for the magnetic resonance and the projection of the magnetic moment along the XY plane rotates at a circular frequency that is equal to the frequency of the applied ac field (Fig. 1). In coordinate system $X'Y'Z$ that rotates at frequency ω of the ac field around the Z axis, vector $\mathbf{M}$ is static or exhibits slow evolution due to transient processes. Components of the moment u and v in the $X'Y'Z$ system are related to components M_X and M_Y: $M_X = u\cos(\omega t)$ and $M_Y = v\sin(\omega t)$. Component M_Z remains unchanged and the same is valid for the magnitude of the transverse component: $M_R = (M_X^2 + M_Y^2)^{1/2} = (u^2 + v^2)^{1/2}$.

Two types of OPQMs employ different types of the magnetic resonance signals. The M_Z magnetometers detect variations in the longitudinal (with respect to the magnetic field) macroscopic magnetization of the

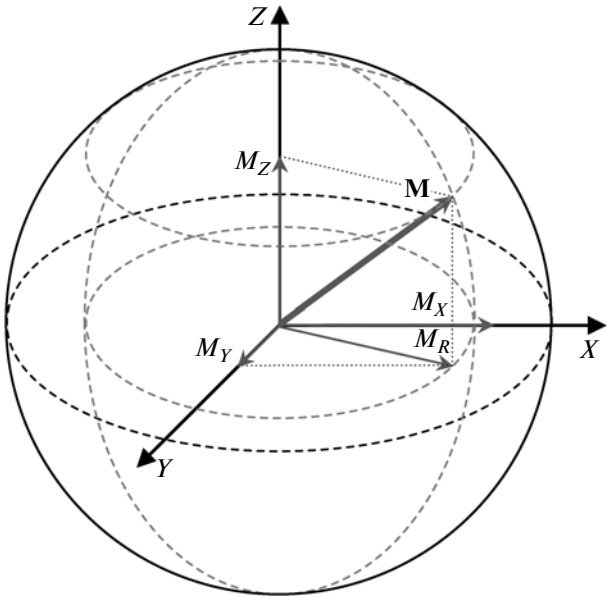

Fig. 1. Bloch sphere and magnetic moment $\mathbf{M}$ in the laboratory coordinates: M_Z longitudinal component of the moment, M_R rotating transverse component, and M_X projection of M_R along the X axis.

atomic medium that is determined by the population of the magnetic Zeeman levels. The M_X magnetometers detect the transverse component of the magnetic moment that oscillates at the Larmor frequency under the exact resonance conditions. Such a signal is related to the induced coherence in the atomic medium that is described using the off-diagonal elements of the density matrix.

Note the substantially different characteristics of the two types of OPQMs. The M_Z magnetometers exhibit a relatively high accuracy that is limited by the shifts of the magnetic resonance line proportional to the linewidth. The operating speed (i.e., the rate at which the magnetic field is measured) is determined by the relaxation time of longitudinal magnetization M_Z, which is also related to the linewidth. Thus, the line narrowing of the magnetic resonance leads to an increase in the accuracy and a simultaneous decrease in the operating speed. The operating speed of the M_Z device is limited by the procedure for the measurement of the center of a symmetric M_Z resonance, which employs the frequency modulation of the resonant RF field at a frequency that is normally lower than the linewidth. The absorption signal is detected at the modulation frequency that is not related to the precession frequency of the magnetic moment and the phase difference between the precessing magnetization and the applied RF field does not affect the measurement accuracy.

The M_X magnetometers exhibit a relatively high operating speed, since the response time is limited by the precession period of magnetic spins, which is several microseconds in the presence of the earth's magnetic field. However, the absolute accuracy of the M_X magnetometer is lower than the accuracy of the M_Z magnetometer due to the externally induced precession of spins in the magnetic resonance. Normally, the external field is the RF magnetic field that is directed perpendicularly or at a certain angle to the measured field. In general, the magnetic resonance can also be excited using the intensity or polarization modulation of the pumping radiation or the modulation of the relaxation time of the medium but such methods are rarely employed in practice. RF field frequency ω is normally controlled with the aid of a phase detector that measures the phase of the M_X-resonance signal relative to the phase of the RF field. In an ideal system, the output signal of the detector is characterized by the dispersion relation with respect to the detuning of the RF field, so that frequency ω and magnetic resonance frequency can be matched.

The dependence of the shape of the detected M_X signal on total phase shift φ in the signal channel of the device is a significant technical problem. Phase shift φ is determined by the physical configuration of the fields that are used in the specific configuration of the M_X magnetometer (i.e., the mutual position of the ac and dc magnetic field vectors with respect to the direction of the pumping and detection radiation) and several technical parameters (e.g., signal delay in electronic circuits).

Phase shift φ is compensated for using phase shifters, and phase compensation accuracy $\Delta\varphi$ is related to absolute error of magnetometer δB: $\delta B = \Gamma \tan(\Delta\varphi)/\gamma$, where Γ is half-width of magnetic resonance line and γ is the gyromagnetic ratio of the OPQM substance. Thus, the measurement error of phase shift φ and variations in this quantity contribute to the magnetometer error. A configuration that is based on the digital technologies in the phase-locked loop of the optically pumped quantum M_X magnetometers is presented in [7], and a method for the analysis of the magnetic resonance signal that allows reliable phase correction in the presence of significant random variations in the magnetic field is proposed in [8]. However, the method implies that the measurements are terminated during the time interval that is needed for the phase-shift correction, so that the procedure cannot be used in the real-time measurements.

An additional significant effect that limits the OPQM accuracy is related to the presence of more than one resonant transition in the low-frequency (Zeeman) spectrum of alkali atoms. In particular, the low-frequency spectrum of the cesium atom in the presence of the earth's mean magnetic field (about 50 μT) contains eight transitions that differ from each other by only about 2 nT. Thus, several resonances merge into one asymmetric resonance with a width of about 14 nT.

As distinct from cesium and remaining alkali metals, potassium exhibits an almost resolved system of magnetic resonances in the ground state in the presence of the earth's magnetic field. Thus, a single line can be selected regardless of the remaining spectral lines and a relatively high limiting accuracy of the potassium magnetometers is achieved. The degree of isolation of the selected resonance depends on the relationship of the linewidth and the distance to the neighboring line. For the M_X signals, the effect of the wing of the neighboring resonance on the peak position of the selected resonance is characterized by quantity $\Delta\omega \cong \alpha\Gamma_2/\Delta$, where $\alpha < 1$ is the relative magnitude of the neighboring resonance, Γ is the width of the resonance, and $\Delta \gg \Gamma$ is the distance to the nearest line. For the M_Z signal, the effect of the neighboring resonance is significantly weaker, since it is proportional to $\Gamma(\Gamma/\Delta)^3$. In the presence of a field of 50 μT, distances Δ are 0.5 and 1.0 kHz for potassium isotopes ^{39}K and ^{41}K, respectively. For a width of resonance of 5 Hz, the frequency shift of the selected resonance due to the effect of the neighboring resonance is less than 0.05 Hz for the ^{39}K isotope. The corresponding maximum measurement error of the magnetic field (about 7 pT) is less than the systematic error of a conventional cesium magnetometer by three orders of magnitude. However, in the presence of a field of 20 μT, the error of the M_X device increases to 44 pT due to the qua-

dratic character of the Zeeman splitting whereas the error of the M_Z device under the same conditions is no greater than 0.17 pT.

Thus, the two types of OPQMs are mutually supplementary with respect to accuracy and operating speed. In the applications that necessitate a relatively high measurement accuracy of the magnetic field, predominantly slow M_Z magnetometers are employed and, vice versa, fast but nonabsolute M_X magnetometers are used in the applications where a relatively high operating speed is more important (e.g., airborne geological survey).

After the pioneer work [9], several variants of the optically pumped magnetometers that combine the advantages of the M_X and M_Z magnetometers were proposed. The main concept employs a combination of two magnetometers in one device, such that the signal of the M_Z magnetometer is used for the slow correction of the fast partner. Then, the concept was implemented in the Cs–K tandem at the Potsdam Geophysical Center [10] and the Cs–4K tandem that employs the signal of the four-quantum resonance in potassium [11]. Such a solution is characterized by higher complexity, since two devices are used instead of one.

FORMULATION OF THE PROBLEM

A variant to solve the problem of the combination of a relatively high sensitivity (typical of the M_Z magnetometer) and a relatively high operating speed (typical of the M_X magnetometer) in the absence of a decrease in the variation sensitivity was proposed in [12]. In this work, we present a detailed description of the scheme. The proposed device is not a tandem if the tandem is interpreted as a structure consisting of two devices with different working substances and/or independent schemes for the optical pumping and detection. To explain the working principle, we employ the theory of magnetic resonance.

We consider a system of magnetic sublevels of the ground state of an alkali atom in the two-level resonance approximation. The optical pumping induces magnetization M_Z that is proportional to the population difference [13]:

$$M_Z = M_Z^0 \frac{\Gamma_2^2 + \delta^2}{\Gamma_2^2 + \delta^2 + 4V^2\Gamma_2/\Gamma_1}. \quad (1)$$

Here, $M_Z^0 = \frac{2}{3}\frac{I}{\Gamma_1} n g_J \mu_B$ is the equilibrium longitudinal magnetization that results from the optical pumping, n is the atomic concentration, g_J is the atomic g factor, μ_B is the Bohr magneton, I is the rate of optical pumping that is proportional to the radiation intensity, Γ_1 and Γ_2 are relaxation constants of the longitudinal and transverse magnetization with allowance for the radiation-induced broadening, $V = g_J\mu_B B_1/\hbar$ is the Rabi frequency of the resonant rotating RF field with amplitude B_1, $4V^2\Gamma_2/\Gamma_1$ is the RF-field-induced broadening, and $\delta = \omega - \omega_0$ is the frequency detuning of radio-field frequency ω relative to the frequency of magnetic resonance $\omega_0 = g_J\mu_B B/\hbar$ in the presence of magnetic field B.

Coherence ρ_{12} that is used to represent oscillating transverse components of magnetic moment M_X and M_Y is given by

$$\rho_{12} = \frac{-iV}{\Gamma_2 + i\delta} N_{21} e^{i\omega t}, \quad (2)$$

$$M_X \propto \mathrm{Re}(\rho_{12})$$

$$= N_{12} g_J \mu_B \frac{-V\delta}{\Gamma_2^2 + \delta^2 + 4V^2\Gamma_2/\Gamma_1} \cos(\omega t), \quad (3)$$

$$M_Y \propto \mathrm{Im}(\rho_{12})$$

$$= N_{21} g_J \mu_B \frac{-V\Gamma_2^2}{\Gamma_2^2 + \delta^2 + 4V^2\Gamma_2/\Gamma_1} \sin(\omega t), \quad (4)$$

where $N_{21} = n(\rho_{22} - \rho_{11})$ is the population difference of the levels.

The signal conversion to the low-frequency range is performed using a phase detector. In general, the output signal of the detector versus detuning δ represents a sum of the dispersion and Lorentzian contours with relative contributions determined by phase φ. It is demonstrated in [7] that a system of two quadrature phase detectors (i.e., detectors whose reference signals are phase-shifted relative to each other by 90°) that generate S_X and S_Y signals can be used for the detection of the signal with the subsequent compensation of the phase shift. Note that the output signals of the detectors can also be represented as sums of two components:

$$S_X(t) \propto \mathrm{Re}[e^{i\varphi}\rho_{12}] = \cos(\varphi) M_X - \sin(\varphi) M_Y, \quad (5)$$

$$S_Y(t) \propto \mathrm{Im}[e^{i\varphi}\rho_{12}] = \cos(\varphi) M_Y + \sin(\varphi) M_X. \quad (6)$$

The summation of components S_X and S_Y with weights of $\cos(\psi)$ and $\sin(\psi)$, respectively, allows to realize a phase shift by arbitrary angle ψ. When $\psi = -\psi$, the resulting signal

$$S = S_X \cos(\psi) + S_Y \sin(\psi) \quad (7)$$

has the dispersion shape $S \sim M_X$. The signal can be used in the scheme of the M_X magnetometer for locking of the RF-field and resonance frequencies. The accuracy (absolute error) of the magnetometer is directly related to the accuracy with which compensating phase ψ is fixed.

Note several methods for the adjustment of compensating phase ψ and measurement of the error of the phase [8]. A common disadvantage of the above methods lies in the fact that the correction of variations in the phase shift cannot be combined with continuous field measurements that are needed in most applications.

A comprehensive solution to the problem that is formulated at the beginning of the section is the implementation of a tandem that employs a single cell and a single magnetic resonance. However, the M_X and M_Z magnetometers are difficult to implement in one sensor, since the two configurations require different positions of the pump and probe beams relative to the magnetic field. In a conventional scheme of the M_X sensor that employs a single beam for pumping and detection of the resonance, the beam is directed at an angle of 45° relative to the magnetic field and both (M_X and M_Z) signals are generated. However, the problems of the simultaneous application are related to different dependences on the angle of the sensor rotation relative to the magnetic field. In addition, the simultaneous detection of the M_X and M_Z signals without a decrease in the signal-to-noise ratio is a nontrivial technical problem. Therefore, the radial (in the XY plane) component of the rotating magnetic moment (M_R signal) is used as a locking signal of the slow precise magnetometer.

The distinctive features of the device are as follows.

(i) Application of radial component M_R of the rotating atomic magnetic moment (Fig. 1).

(ii) Combination of a continuously working fast M_X magnetometer and a precise slow M_R magnetometer that work using the same atoms and a single radio optical scheme. As in the tandem schemes of [10, 11], the signal of the slow precise magnetometer is used for the correction of the signals of the fast M_X magnetometer.

(iii) Implementation of the device based on the conventional potassium M_X sensor with modifications only concerning the parts responsible for the processing of the magnetic resonance signal.

PRACTICAL IMPLEMENTATION OF THE M_X–M_R MAGNETOMETER

Using the same quadrature phase detectors (expressions (5) and (6)), we supplement the detection of the M_X signal with the measurement of the squared magnitude of transverse component $\mathbf{M}_R = M_X\mathbf{e}_X + M_Y\mathbf{e}_Y$ of the rotating moment:

$$M_R^2 = M_X^2 + M_Y^2 = S_X^2 + S_Y^2. \quad (8)$$

Note that the result of the measurement does not depend on phase φ, since the magnitude of the vector is independent of the coordinate system in which it is determined. The squared M_R signal quadratically depends on detuning δ:

$$\mathbf{M}_R^2 = (M_Z^0)^2 V^2 \frac{\Gamma_2^2 + \delta^2}{(\Gamma_2^2 + \delta^2 + 4V^2\Gamma_2/\Gamma_1)^2}. \quad (9)$$

Signal M_R^2 is symmetric in terms of detuning δ, and the Lorentzian dependence on the detuning (similar to the signal of the M_Z magnetometer) is obtained when the RF-field-induced broadening is relatively small ($V \longrightarrow 0$). Note also that the weakness of the effect of the neighboring resonances on the peak position of the M_R^2 signal is the same as for the M_Z signal. With allowance for the fact that the M_R^2 signal is independent of phase φ, we can find the exact position of the magnetic resonance frequency and, hence, determine the correct compensating phase ψ.

As in the case of the M_Z magnetometer, it is expedient to employ the detuning modulation $\delta_M = \delta + \varepsilon\sin(2\pi\Omega t)$ at a relatively low frequency Ω with deviation ε. At nonzero detuning δ, signal M_R^2 is modulated at frequency Ω. The lock-in detection at this frequency makes it possible to obtain the low frequency error signal for $M_R'^2$ that is an odd function of detuning δ when the modulation is slow in comparison with the resonance width:

$$M_R'^2 = 2(M_Z^0)^2\delta\varepsilon V^2 \frac{4V^2\Gamma_2/\Gamma_1 - \Gamma_2^2 - \delta^2}{(\Gamma_2^2 + \delta^2 + 4V^2\Gamma_2/\Gamma_1)^3}. \quad (10)$$

The modulation at frequency Ω vanishes when the radio-field frequency is exactly tuned (δ = 0).

Below, we consider the dependence of the $M_R'^2$ signal on the phase error $\Delta\varphi = \varphi - \psi$, which is related to the detuning in the closed feedback (FB) loop:

$$\delta = \Gamma\tan(\Delta\varphi). \quad (11)$$

Here, $\Gamma = \sqrt{\Gamma_2^2 + 4V^2\Gamma_2/\Gamma_1}$ is the total width of the resonance.

Figure 2 presents the block diagram of the magnetometer, which differs from that in [7] only by the software algorithm. We cannot rapidly (at times $t < T_{\mathrm{mod}}$) measure the frequency in the scheme of the M_X magnetometer if the resonant radio-field frequency is directly modulated (as in the M_Z scheme). To simultaneously perform fast (M_X channel) and slow (M_R channel) measurements, we employ the modulation of the locking level of the M_X magnetometer with respect to S signal (7) instead of the modulation of frequency detuning δ.

In a conventional M_X magnetometer the FB loop (FB1) is aimed at satisfying equality $S = 0$. We change the FB1 parameters in such a way that signal S tends to levels $-L$ and $+L$ over the first and second halves of period T_{mod}, respectively. Thus, we perform rectangular (accurate to FB1 time constant) modulation of both frequency detuning δ and phase shift Δφ, so that the M_X magnetometer, whose operating speed is higher than the modulation frequency by two-to-three orders of magnitude, detects variations in the magnetic field at any time interval inside the modulation period. Resulting readings $f_i(t)$ of the M_X magnetometer are modulated at the low frequency $\Omega = 1/T_{\mathrm{mod}}$. The second FB (FB2) selects the signal at frequency Ω from

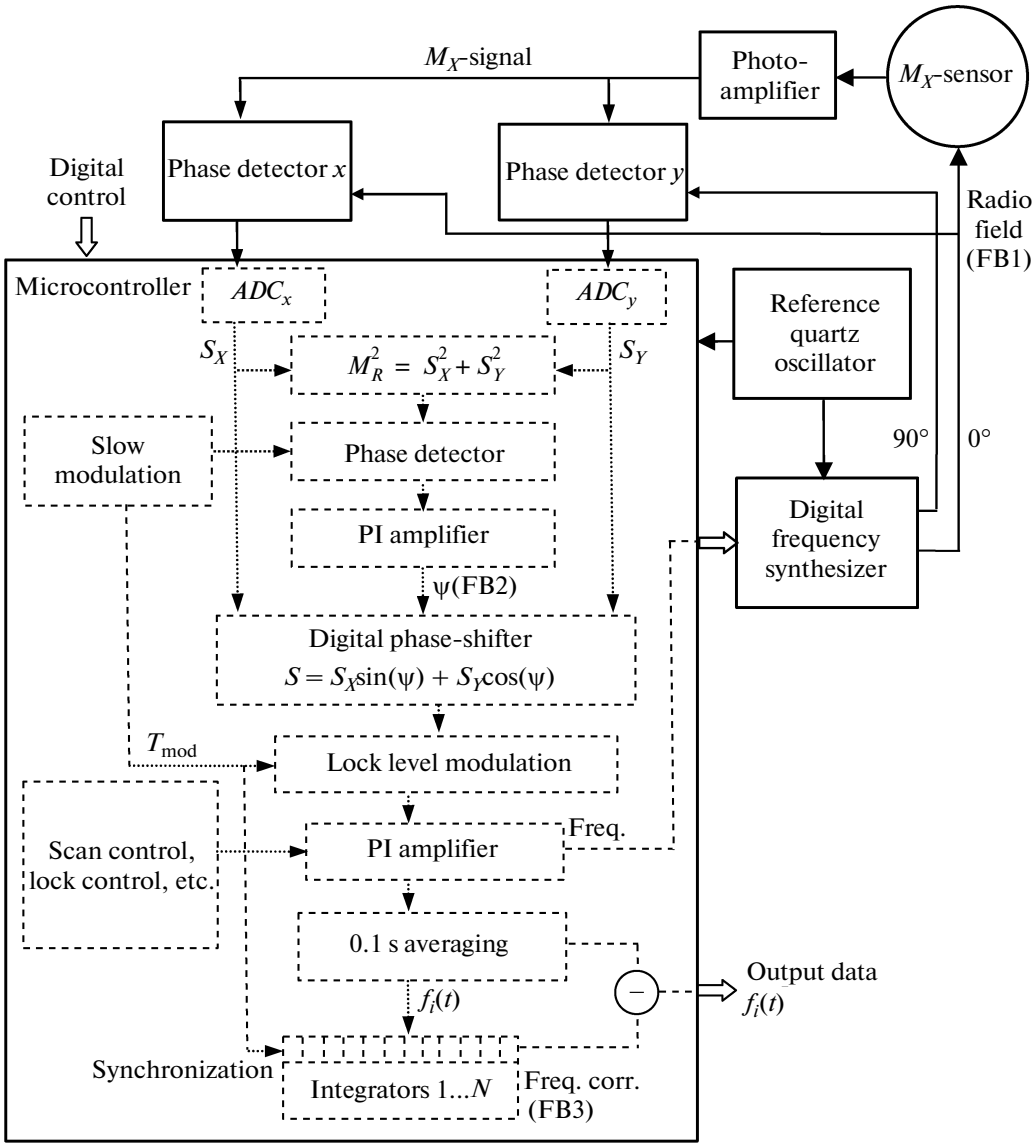

Fig. 2. Block diagram of the M_X–M_R magnetometer.

the magnetometer output and employs it as an error signal that controls compensating phase ψ.

The effects that determine the shifts of the OPQM readings can be divided into two classes: (i) shifts of the position of the magnetic resonance related to the pumping parameters and the properties of the working medium of the magnetometer and (ii) systematic measurement errors of the magnetic resonance frequency related to the parameters of electro-optical and electronic elements and circuits of the magnetometer and the configuration of the sensor.

Note also that FB2 allows the compensation of only systematic errors of the second type.

The third FB (FB3) is implemented to eliminate the modulations in the output signal of magnetometer $f_i(t)$. For this purpose, a regular component that is related to the modulation at frequency Ω is selected in the output data at a relatively large number of periods, stored in memory, and, then, subtracted.

EXPERIMENT

For the verification of the concept of the M_X–M_R magnetometer, we employ the potassium M_X sensor with combined pump and probe beams and the digital FB circuit from [7]. We perform the measurements in a magnetic shield in the presence of a field of about 45 μT in the absence and in the presence of the magnetic field stabilization. The field in the shield is measured using the M_Z magnetometer. The half-width of the M_X resonance line at optimal pumping intensity is 0.9 nT (6.3 Hz), and a variation sensitivity of the M_X magnetometer is 0.5 pT at a measurement time of 0.1 s.

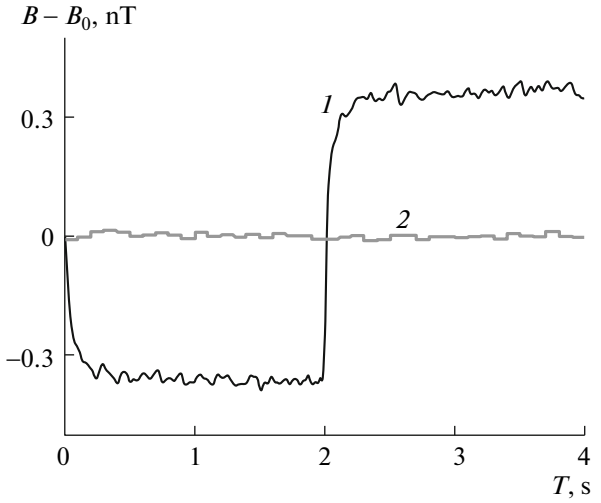

Fig. 3. Time dependence of the output signal of the magnetometer for modulation period $T_{mod} = 4$ s in the presence of the stabilized field: (*1*) prior to correction (output at 1280 counts/s) and (*2*) after averaging over 0.1 s and correction.

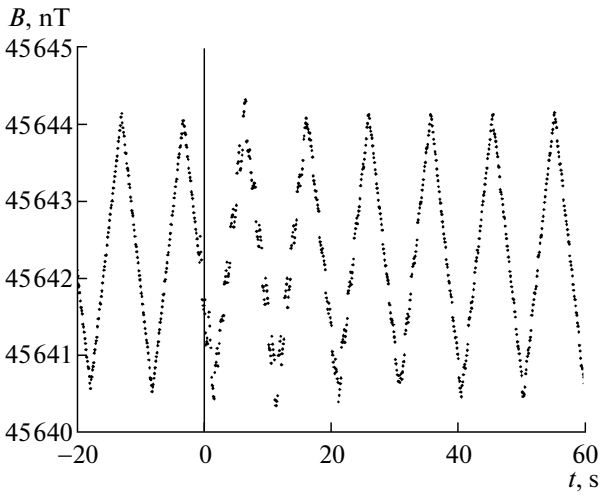

Fig. 4. Output signal of the device in the presence of the modulated magnetic field for the M_R channel switched on at $t = 0$.

The FB1 time constant is $\tau_1 \sim 10^{-4}$ s. The software algorithm of the digital FB is modified in accordance with Fig. 2. Modulation period T_{mod} ranges from 1 to 4 s, so that inequalities $T_{mod} \gg 1/\Gamma_1$ and $1/\Gamma_2$ are satisfied, and, finally, we employ $T_{mod} = 1$ s. The FB2 and FB3 time constants are determined by the software proportional integral controllers in interval 25–150 s.

For the data output rate $n = 10$ s^{-1}, we implement $N = nT_{mod} = 10$ software registers that accumulate data on the modulation of the output signal of the magnetometer by the FB3 loop for the subsequent correction. Figure 3 shows the time dependence of the output signals of the device at $T_{mod} = 4$ s prior to correction (curve *1*) and after averaging at $1/n = 0.1$ s and correction (curve *2*).

When the above method for the elimination of the modulation in the output signal is implemented, the system is insensitive to the spectral components in the frequency band $1/T_{md} \pm 1/(2\pi\tau_3)$, where τ_3 is the FB3 time constant. The modulation of the output signal of the magnetometer depends on longitudinal relaxation time T_1 and parameters of the FB1 loop. Therefore, time constant τ_3 is bounded from above by variation times of the FB1 parameters, which can be relatively large (up to several hundreds of seconds), and the width of the blind interval is relatively small.

Figure 4 demonstrates the efficiency of the system. The time-dependent magnetic field is exerted on the device, the M_R channel is switched off prior to moment $t = 0$, and the device works as the M_X magnetometer. The FB2 and FB3 loops of the M_R channel are activated at $t = 0$, and the output signals are initially modulated with a period of 1 s. The modulation vanishes with a delay of several tens of seconds due to the effect of the FB3 loop.

Figure 5 demonstrates the dependence of the response of the device on the perturbation frequency of the magnetic field. As was expected, the device is insensitive to field variations at a frequency of 1 Hz. The inset shows that the width of the dip at a frequency of 1 Hz depends on τ_3. We assume that the specific features at frequencies of 2, 3, ..., n Hz and in the vicinity of these frequencies can be eliminated using the sine-shaped modulation of the locking frequency instead of the rectangular modulation.

The absolute accuracy of the M_X magnetometer is primarily determined by the accuracy of compensating phase ψ. The phase accuracy in the M_X–M_R mag-

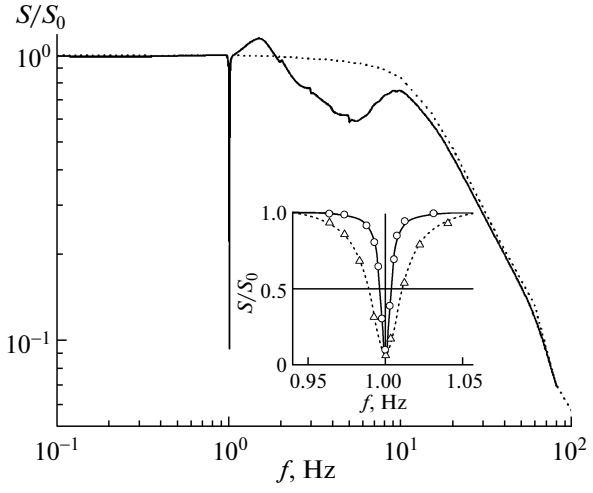

Fig. 5. Frequency response functions of the magnetometer for (dashed line) M_X and (solid line) M_X–M_R regimes. The inset shows an interval in the vicinity of a frequency of 1 Hz for FB3 time constants of 37 and 133 s.

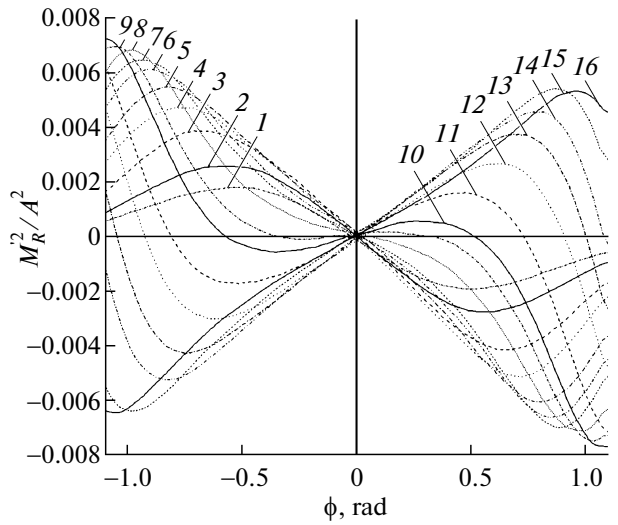

Fig. 6. Plots of the $M_R'^2$ signal vs. phase mismatch for several amplitudes of the resonant RF field (the numbers on the curves correspond to the dot numbers in Fig. 7).

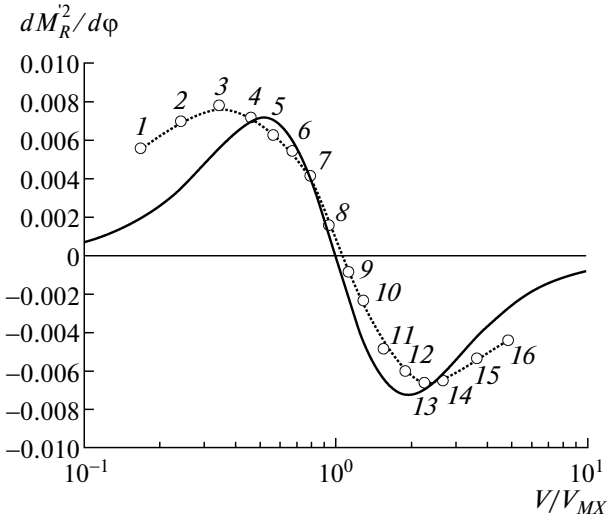

Fig. 7. Plots of the slope of the M_R^2 signal vs. amplitude of the resonant RF field V: (solid line) theoretical data and (dashed line) result of the approximation of the experimental data.

netometer is proportional to the slope of the demodulated $M_R'^2$ signal.

The maximum slope of the $M_R'^2$ signal is reached at the Rabi frequency of the resonant RF field V_{MR} that satisfies the condition $V_{MR} = 1/2\sqrt{2-\sqrt{3}}\,(\Gamma_1\Gamma_2)^{1/2} \cong 0.259(\Gamma_1\Gamma_2)^{1/2}$. This value is approximately two times less than the optimal value for the M_X magnetometer $V_{MX} = 1/2(\Gamma_1\Gamma_2)^{1/2}$. Note that the slope of the $M_R'^2$ signal is zero at $V = V_{MX}$ (Figs. 6, 7).

Figure 6 presents the dependences of the M_R^2 signal on the phase mismatch for several amplitudes of the resonant RF field. The results of the measurements are used to plot the slope of the M_R^2 signal versus the amplitude of the resonant RF field (Fig. 7). Each dot in Fig. 7 corresponds to a curve in Fig. 6. Presumably, the difference between the experimental curve and the theoretical predictions is due to the systematic error in the measurement of effective field V.

We also optimize modulation frequency Ω and frequency deviation ε with respect to total half-width Γ. The problem was theoretically solved for the two-level atom using the nonstationary perturbation theory: for the rectangular frequency modulation $\delta_M = \delta + \varepsilon\,\mathrm{sgn}[\sin(2\pi\Omega t)]$, the calculation in the first order of the perturbation theory yields $\Omega = 0.206\Gamma$ and $\varepsilon \approx 0.586\Gamma$. The experimental values $\Omega = 1$ Hz $\sim 0.16\Gamma$ and $\varepsilon \sim 0.5\Gamma$ are close to the calculated results.

For the direct estimation of the reproducibility of the magnetometer results, we employ multiple measurements of the stabilized phase. This quantity is measured with a delay of about 3000 s that is sufficient for the processing of the perturbation in the FB2 loop. Seventy-five measurements are performed in the magnetic shield in the presence and in the absence of the stabilization of the magnetic field. The duration of each independent measurement is 2400 s. The FB2 time constant is 120–150 s, so that each measurement is divided into 20 intervals of 120 s. We assume that stabilized phases ψ at the intervals are mutually independent. Each series of 20 measured values is used to calculate variance σ and Allan variance σ_A of the phase. The Allan variance allows significant suppression of the monotonic variations and provides the characteristic variation in the measured parameter over a time interval of 120 s. Magnetometer error σ is determined from phase variation $\delta\varphi$ using expression (11).

The statistical estimate of the reproducibility of the stabilized phase using 75 arrays consisting of twenty 120-s-long measurements corresponds to the statistical estimate of the reproducibility of the M_X–M_R magnetometer $\sigma = 1.2 \pm 1.1$ pT, whereas the Allan variance for the same measurements is $\sigma_A = 0.32 \pm 0.13$ pT. The fact that the regular variance is greater than the Allan variance can be due to the temperature dependence of the phase shift at times of greater than 120 s: the measurements show that the shift recalculated in the magnetic field units is 3–6 pT/°C for the temperature changes inside the sensor. As was mentioned, such an intrinsic phase shift of the M_X magnetometer is measured and compensated by using the FB2 loop.

CONCLUSIONS

We proposed and experimentally tested a scheme of the optically pumped quantum M_X–M_R magnetome-

ter in which the conventional fast M_X magnetometer is supplemented with the precise slow M_R magnetometer that employs the same atoms, the same optical scheme, and uses the radial component of the rotating atomic magnetic moment as the locking signal. A sampling rate of 10 counts/s is demonstrated when the statistical estimate of reproducibility is 1.2 ± 1.1 pT and the Allan variance is 0.32 ± 0.13 pT over a time interval of 120 s that is equal to the feedback constant in the system for the correction of the phase shift.

ACKNOWLEDGMENTS

This work was supported by the Ministry of Education and Science of the Russian Federation.

REFERENCES

1. W. Happer, Rev. Mod. Phys. **44**, 169 (1972).
2. E. B. Aleksandrov and A. K. Vershovskii, Phys. Usp. **52**, 573 (2009).
3. D. Budker and M. V. Romalis, Nature Phys. **3**, 227 (2007).
4. A. Kastler, J. Phys. Radium **11**, 255 (1950).
5. A. Kastler, J. Opt. Soc. Am. **47**, 460 (1957).
6. F. Bitter, Phys. Rev. **76**, 833 (1949).
7. A. K. Vershovskii and A. S. Pazgalev, Tech. Phys. **51**, 924 (2006).
8. A. K. Vershovskii and E. B. Aleksandrov, Opt. Spectrosc. **100**, 12 (2006).
9. A. H. Allen and P. L. Bender, J. Geomagn. Geoelectr. **24**, 105 (1972).
10. E. Pulz, K.-H. Jackel, and H.-J. Linthe, Meas. Sci. Technol. **10**, 1025 (1999).
11. E. B. Aleksandrov, M. B. Balabas, A. K. Vershovskii, and A. S. Pazgalev, Tech. Phys. **45**, 931 (2000).
12. A. K. Vershovskii and A. S. Pazgalev, Tech. Phys. Lett. **37**, 23 (2011).
13. F. Bloch, Phys. Rev. **70**, 460 (1946).

Translated by A. Chikishev